Local strain-induced band gap fluctuations and exciton localization in aged WS_2 monolayers

J. Krustok, R. Kaupmees, R. Jaaniso, V. Kiisk, I. Sildos, B. Li, and Y. Gong

Citation: AIP Advances **7**, 065005 (2017); doi: 10.1063/1.4985299
View online: http://dx.doi.org/10.1063/1.4985299
View Table of Contents: http://aip.scitation.org/toc/adv/7/6
Published by the American Institute of Physics

Local strain-induced band gap fluctuations and exciton localization in aged WS_2 monolayers

J. Krustok,[1,2,a] R. Kaupmees,[2] R. Jaaniso,[3] V. Kiisk,[3] I. Sildos,[3] B. Li,[4] and Y. Gong[5]

[1]*Division of Physics, Tallinn University of Technology, Ehitajate tee 5, 19086 Tallinn, Estonia*
[2]*Department of Materials and Environmental Technology, Tallinn University of Technology, Ehitajate tee 5, 19086 Tallinn, Estonia*
[3]*Institute of Physics, University of Tartu, W. Ostwaldi 1, 50411 Tartu, Estonia*
[4]*Department of Mechanical Engineering, Villanova University, 800 Lancaster Avenue, Villanova, Pennsylvania 19085, USA*
[5]*Department of Materials Science and Engineering, Stanford University, Stanford, California 94305, USA*

(Received 11 April 2017; accepted 26 May 2017; published online 5 June 2017)

Optical properties of aged WS_2 monolayers grown by CVD method on Si/SiO_2 substrates are studied using temperature dependent photoluminescence and reflectance contrast spectroscopy. Aged WS_2 monolayers have a typical surface roughness about 0.5 nm and, in addition, a high density of nanoparticles (nanocaps) with the base diameter about 30 nm and average height of 7 nm. The A-exciton of aged monolayer has a peak position at 1.951 eV while in as-grown monolayer the peak is at about 24 meV higher energy at room temperature. This red-shift is explained using local tensile strain concept, where strain value of 2.1% was calculated for these nanocap regions. Strained nanocaps have lower band gap energy and excitons will funnel into these regions. At T=10K a double exciton and trion peaks were revealed. The separation between double peaks is about 20 meV and the origin of higher energy peaks is related to the optical band gap energy fluctuations caused by random distribution of local tensile strain due to increased surface roughness. In addition, a wide defect related exciton band X_D was found at about 1.93 eV in all aged monolayers. It is shown that the theory of localized excitons describes well the temperature dependence of peak position and halfwidth of the A-exciton band. The possible origin of nanocaps is also discussed. [http://dx.doi.org/10.1063/1.4985299]

I. INTRODUCTION

Layered semiconductor compounds involving transition metals from group VI and chalcogens (TMDs) are promising candidates for studying atomically thin structures and have attracted considerable attention because of their unique properties and their potential applications in various opto-electronic devices.[1] The basic building block of these layers consists of one atomic layer of transition metal atoms sandwiched by two chalcogen atomic layers, thus forming one monolayer. All these monolayers have a strong intra layer chalcogen-metal covalent bond while different layers are weakly linked by van der Waals forces. These binary compounds are typically semiconductors with an indirect band gap, while monolayers often have a direct band gap in the visible or near infrared spectral range. The band gap energy of WS_2 bulk crystals is about 0.88 eV, while the monolayer shows an optical bandgap around 2.0 eV.[2] Optical properties of WS_2 monolayers have been studied in many papers.[3–14] The room temperature photoluminescence (PL) spectrum of the WS_2

[a]E-mail: Juri.Krustok@ttu.ee

monolayer is characterized by the presence of two exciton peaks that arise from vertical transitions at the K point of the Brillouin zone from a spin-orbit-split valence band to a nearly degenerate conduction band. These PL peaks are called as A and B peaks with peak positions near 2.0 and 2.4 eV, respectively.[15] So the spin-orbit splitting of the valence band is found to be 425 meV in WS_2 monolayer.[16] Besides a neutral A^0 exciton peak a trion (A^-) peak is often visible at about 43 meV lower energy.[11] At temperatures below T=80K the trion peak usually dominates. However, the actual peak positions of excitons and trions are very sensitive to the preparation method of monolayers. Often monolayers grown by chemical vapor deposition (CVD) on Si/SiO_2 substrates show PL emission at lower energies with respect to monolayers transferred by mechanical exfoliation from bulk crystals or monolayers grown on other substrates.[17,18] The main reason of this redshift is believed to be related to the strain in as-grown monolayers, which is usually released after the monolayer is transferred on the same Si/SiO_2 substrate.[5,19] It was found that the uniaxial tensile strain could cause the red shift of A-exciton peak in WS_2 monolayer at a rate –11.3 meV per % of strain.[5] However, slightly higher values were predicted by theoretical calculations.[19] The origin of the strain in as-grown monolayers is due to the different thermal expansion coefficients (TEC) of WS_2 and SiO_2 substrate. But additional strain could be related to the surface roughness, which is causing a local strain depending on a surface topography. In MoS_2 monolayers this concept was verified by creating artificial atoms[20] or wrinkles[21] on a substrate surface and thus getting very high values of local tensile strain and, accordingly, band gap energy fluctuations. The formation of quite high wrinkles in WS_2 monolayers due to strain relaxation processes was recently reported[22] and the A^0 band was red-shifted in these wrinkled areas due to layer bending. Even in WS_2 monolayers prepared by mechanical exfoliation there is a remarkable inhomogeneous strain across the monolayer's area and spatial non-uniformity of the electron density across the monolayer surface due to oxygen chemisorption.[23] Besides a strain many structural defects exist in CVD-grown WS_2 on Si/SiO_2. These defects introduce localized states in the bandgap, leading a dramatic decrease in the carrier mobility. It was found that CVD-grown monolayer of WS_2 on Si/SiO_2 substrate shows about 10^3 times lower carrier mobility than mechanically exfoliated samples measured under similar conditions.[24,25] It was also reported, that during CVD growth S-rich and S-poor domains could be formed within WS_2 monolayers with very different properties and this could be also one possible reason of spatial non-uniformity of WS_2 monolayers.[26]

Majority of TMD studies were performed on fresh grown monolayers and usually all these compounds have been considered as air-stable semiconductors under ambient conditions. However, recent studies show that CVD grown TMD monolayers exhibit not so good long-term stability in air and usually large-scale structural and morphological changes can be detected after about 1 year storage at normal laboratory atmosphere.[27] The presence of oxidized metal states and organic adsorbates were detected in aged MoS_2 and WS_2 monolayers. The degradation of monolayers commonly starts from grain boundaries and these oxidation processes can be accelerated by using higher temperatures.[28] Unfortunately, optical properties of aged TMD monolayers have not been studied in detail so far. However, it was reported that the PL intensity of aged WS_2 monolayers grown on sapphire substrate drops noticeably and shows large spatial variations.[27]

In our recent paper[29] optical properties of aged $MoSe_2$ monolayers were studied. These monolayers showed quite high surface roughness leading to a random distribution of local tensile strain and, thus, spatial optical band gap energy fluctuations. Local band gap minimums are capable of efficient funneling and localization of excitons. It was shown that the model of localized excitons describes well the shape and temperature dependence of excitonic PL band. It is obvious that aging of TMD monolayers is quite complicated and different monolayers can show very different behavior. Therefore aging processes and their effect on optical properties of different TMD monolayers definitely need further studies to clarify the nature aging and to understand exciton localization routes.

In the present work we provide new and additional to Ref. 29 experimental results on optical properties of CVD grown and aged WS_2 monolayers on Si/SiO_2 substrates. We show that also aged WS_2 monolayers exhibit different local strains due to surface topography leading to excitons localization.

II. EXPERIMENTAL DETAILS

An original tellurium-assisted CVD method was used to synthesize WS_2 layers on Si/SiO_2 substrate under atmospheric pressure in a quartz reaction tube (inner diameter ~ 5 cm). For WS_2 synthesis, mixed W and Te powders were scattered on a Si/SiO_2 substrate. The quartz tube was heated to 500 °C at a rate of 50 °C/min and was then kept at 500 °C for 15 min before cooling. Using W/Te precursor allows growth at temperatures much lower when compared to that of CVD syntheses using WO_3 precursors (~800 °C). The sulfur powder was loaded at the upstream zone inside the same quartz tube with a temperature of about 200 °C. Argon (100 sccm) was used as protection from oxidation and carrier gas during growth. No tellurium containing phases were detected after growth in WS_2 layers. More details of the growth process can be found in the paper by Y. Gong et al.[12] WS_2 monolayers used in this study were stored in air under ambient conditions (i.e., room temperature and atmospheric pressure) for about 1 year.

Raman, reflectance contrast (RC) and μPL measurements were carried out using a Horiba LabRAM HR800 Micro-Raman system or a Renishaw inVia Raman microscope (through 50x or 100x objective lenses) equipped with a multichannel CCD detection system in the backscattering configuration with a spectral resolution better than 1 cm^{-1}. An Nd-YAG laser (wavelength 532 nm) or an Ar laser (wavelength 488 nm) was used for excitation. The laser spot size was about 2 μm in diameter. Linkam THMS350V heating/cooling stage was used for temperature dependent Raman measurements (T=80-300K). For the low temperature (T=10-300K) PL and RC measurements, the UTREKS-LSO cryosystem with the helium-bath cryostat was used. An atomic force microscope (AFM; Bruker Multimode) with a Nanoscope V controller was used to determine the surface roughness and the thickness of the layers.

III. RESULTS AND DISCUSSION

A. General properties

The WS_2 monolayers mainly grow as triangular islands with domain sizes up to tens of micrometers (see Fig. 1 (a) (b)). There are also regions where additional 2L and even 3L layers can be observed in the center of some triangles. The thickness of as-grown WS_2 monolayers was measured with AFM and was about 0.8 nm and the sample surface was quite smooth (surface roughness ~0.3 nm).[12] On the contrary, aged WS_2 monolayers have a typical surface roughness about 0.5 nm and, in addition, a high density of nanocaps with the base diameter about 30 nm and average height of 7 nm, see Fig. 1(c). Similar nanocaps were found also in aged $MoSe_2$ monolayers.[29]

Figure 2 shows the Raman spectra of aged WS_2 monolayer at different temperatures. All Raman spectra measured from different monolayer islands are quite similar and do not differ significantly from the spectra of as-grown layers. The frequency separation of ~60 cm^{-1} between $E^1_{2g}(\Gamma)$ and $A_{1g}(\Gamma)$ modes is typical for single layer WS_2 measured in many papers.[30–33]

At the same time the μPL spectrum of aged WS_2 monolayer is red-shifted about 24 meV, see Fig. 3. It is known that the PL peak position of TMD monolayers is very sensitive to the strain and often CVD grown monolayers show exciton emission at lower energy than monolayers transferred by mechanical exfoliation from bulk crystals. It has been shown that the thermal expansion coefficient (TEC) of WS_2 is smaller than that of the Si/SiO_2 substrate.[34] Therefore, we will expect an in-plane compression stress on WS_2 during cooling after CVD growth and, finally, formation of tensile strain. It was found[19] that the strain affects a band gap energy and also a work function of WS_2. Often this compressive stress leads to formation of ripples and other local inhomogeneities with different strain values. As it was shown[19] the tensile stress (positive strain) has higher effect on the band gap energy than the compressive stress (negative strain). So it is natural to believe that in our aged monolayers some additional tensile strain is causing this 24 meV red-shift of exciton PL peak and the origin of this extra strain seems to be related to observed nanocaps.

The room temperature μPL spectrum of aged monolayer showed only one slightly asymmetric A-exciton peak. Completely different spectra were obtained at T=10K, see Fig. 4, where 5 different PL bands can be clearly observed. All spectra were fitted using an asymmetric hyperbolic secant function $I(E) = I_0\left[e^{(E-E_M)/W_{HE}} + e^{-(E-E_M)/W_{LE}}\right]^{-1}$ and the result of this fitting for one spectrum is also shown

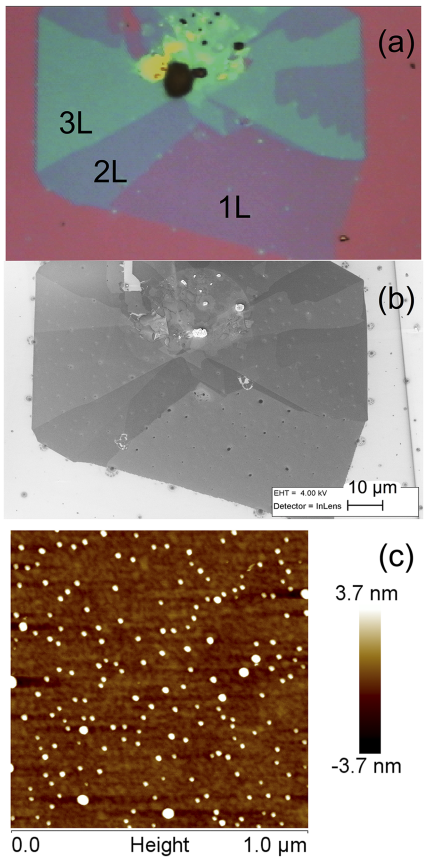

FIG. 1. Optical (a) and SEM (b) microscopy images of WS_2 layers on Si/SiO_2 substrate. The positions of single layer (1L), double (2L) and triple (3L) layers were indicated, (c) the AFM scan from the 1L area.

in Fig. 4. Here W_{HE} and W_{LE} are related to the width of high energy and low energy sides of the PL band, respectively, while E_M is related to the peak position $E_{max} = E_M - \left[\frac{W_{HE}W_{LE}}{W_{HE}+W_{LE}}\right] ln\left(\frac{W_{LE}}{W_{HE}}\right)$, but only in case of symmetrical band $E_M = E_{max}$. The hyperbolic secant function is found to fit well also excitonic PL bands in $MoSe_2$ monolayers.[35] Somewhat altered shape and intensity

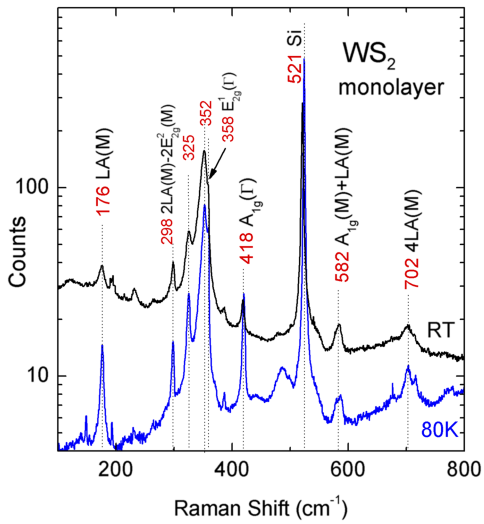

FIG. 2. Room temperature (black) and low temperature (T=80K) (blue) Raman spectra from a WS_2 monolayer region.

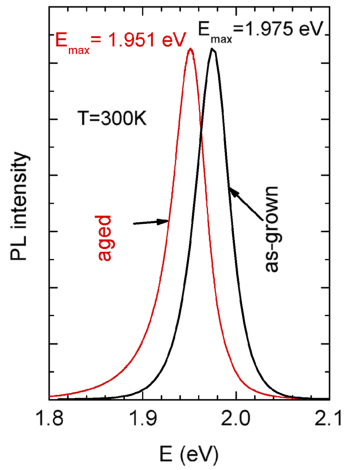

FIG. 3. Normalized room temperature PL spectra of as-grown and aged WS_2 monolayers. The separation between PL peaks is 24 meV.

of the spectra taken from different islands and different positions demonstrate large spatial variations of monolayers properties. At the same time peak positions of all PL bands (except X_D) remained almost constant. All PL bands can be divided into 3 groups: A-exciton peaks A^0 (E_{max} = 2.030 eV) and A_S^0 (E_{max} = 2.010 eV); trion peaks A^- (E_{max} = 1.989 eV) and A_S^- (E_{max} = 1.970 eV), and a deep defect related exciton peak X_D (E_{max} = 1.93 eV). Here the subscript S denotes shallow states. The double structure of exciton and trion peaks is rather extraordinary and can be seen merely at very low temperatures (T < 30K). At higher temperatures only A^0 and A^- peaks together with X_D peak persist. The separation between double peaks is about 20 meV. The origin of these peaks will be further discussed later. Rather high intensity of defect related exciton peak X_D in all monolayer islands is a clear indication of high concentration of defects in aged WS_2 monolayers. We also observed that the high intensity of X_D peak is usually accompanied by the high intensity of trion peak.

Figure 5 presents the PL spectra of aged WS_2 monolayer measured at T=80K using different laser power. All spectra were fitted with an asymmetric hyperbolic secant function and the fitting result for 3.5 μW spectrum is presented as blue and red lines. The inset shows the integrated intensities of A^0, A^- and X_D bands as functions of the excitation power. With the increase in the excitation power, the emission from exciton and trion states linearly increases (slope = 1) over the whole studied range.

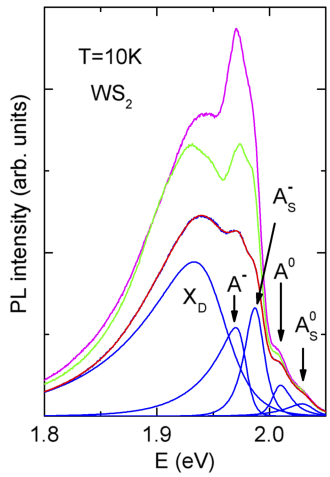

FIG. 4. Low temperature (T=10K) μPL spectra of WS_2 monolayer island taken from 3 different spots. Result of spectral fitting with an asymmetric hyperbolic secant function is also shown for one spectrum.

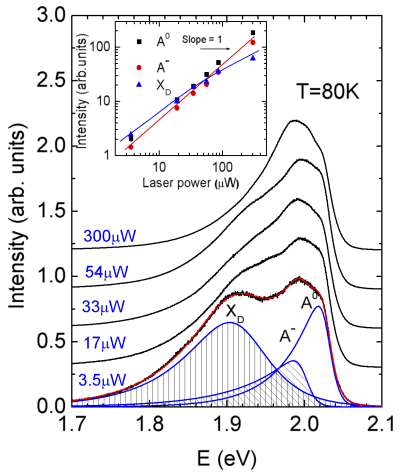

FIG. 5. Excitation intensity dependent normalized PL spectra of aged monolayer WS_2 measured at T=80K and a result of fitting with asymmetric hyperbolic secant function. All spectra are vertically shifted for clarity. The inset shows the integrated intensity of different peaks as a function of laser power.

The emission from X_D shows a sublinear dependence and saturates at higher excitation power. Similar saturation of the wide X_D band was observed also in MoS_2[36] and in other WS_2 monolayers.[10] The nature of defects responsible for the X_D band is not clear, but due to very wide and somewhat variable shape of this band we can expect a presence of several different defects.

B. Temperature dependence

For temperature dependent RC and μPL measurements we selected monolayer regions, where low-temperature PL intensities of X_D and trion bands were lowest and, thus, the shape of the A^0 band is more or less well defined. Unfortunately at temperatures T < 80K the X_D and trion bands started to appear and the reliability of PL spectral fitting suffers a lot. This was not a case with RC measurements, where spectra were unaffected by trion resonances even at very low temperatures, see Fig. 6 (a). If $R(E)$ and $R_0(E)$ are the reflectance spectra of the WS_2 monolayer and the Si/SiO_2 substrate respectively, as a function of the photon energy (E), then the RC spectrum is defined as

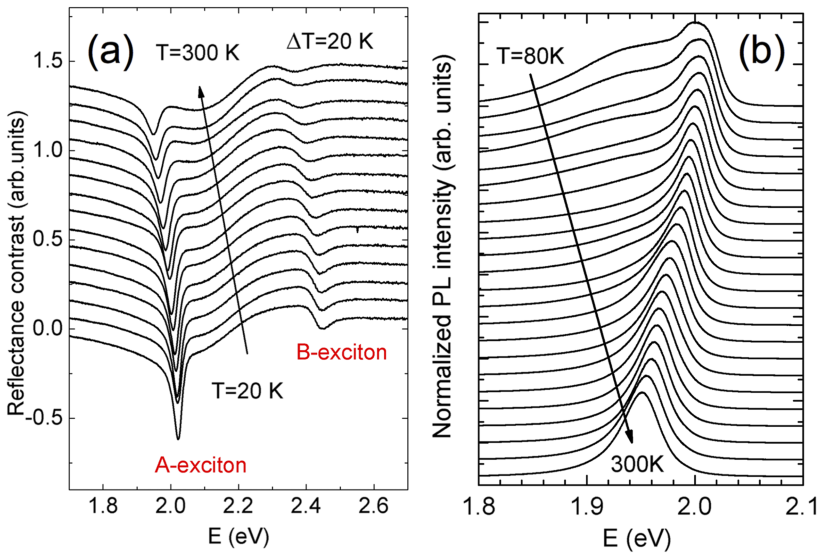

FIG. 6. (a) Temperature dependence of the reflectance contrast spectra of aged WS_2 monolayer showing A and B exciton resonances. (b) Temperature evolution of normalized A^0-exciton PL emission.

follows: $RC(E)=[R(E) - R_0(E)]/[R(E)+R_0(E)]$. As it was shown[37] the inverted reflectance contrast spectra of 2D monolayers near the exciton resonances are usually proportional to the absorption and therefore the shape of inverted RC can be used to probe the density of excitonic states. For the RC peak fitting we used again the asymmetric hyperbolic secant function after subtracting slowly changing background. The asymmetric hyperbolic secant function was used because RC peak had an asymmetric shape with larger width at low energy side. The ratio W_{LE}/W_{HE} was about 2.5 and did not change with temperature. Both, A and B exciton peaks were detected. The same fitting function was used also for μPL spectra, presented in Fig. 6 (b). Values for peak position E_{max} and full width at half maximum ($FWHM$) for A^0 -exciton peaks were calculated numerically from fitting curves and are presented in Fig. 7.

The temperature dependence of A^0-exciton peak position obtained from RC measurements can be well described by a standard semiconductor bandgap model:[38]

$$E_{\max} = E(0) - S\hbar\omega[\coth(\hbar\omega/2kT) - 1], \tag{1}$$

where $E(0)$ is a peak position at T= 0K, S is dimensionless electron-phonon coupling strength and $\hbar\omega$ is an average phonon energy. The fitting result with Eq. (1) is shown as a red line in Fig. 7(a) and parameters found from fitting are given in Table I. Very similar behavior is seen also for B peak, see Fig. 7(a). The separation between A and B exciton peaks is ~420 meV and this value is very close to the spin-orbit splitting of the valence band 425 ± 18 meV found for WS_2.[16] Actually, these fitting parameters are comparable with parameters for WS_2 monolayers obtained by mechanical exfoliation from a bulk crystal and without any strain.[3] However, some discrepancies also exist between the parameters. First, $E(0)$ values differ about 42 meV. Second, the A^0 exciton peak position found from PL measurements has slightly different behavior, see Fig. 7(a). At lower temperatures the separation between A^0 exciton peaks measured using reflectance contrast (absorption) and PL is increasing and this is typical for localized excitons, where the temperature dependence of peak position often exhibits an S-shape behavior.[39,40]

Figure 7(b) shows the temperature dependence of the full width at half maximum ($FWHM$) of A-exciton line found from reflectance contrast and PL spectra. The linewidth broadening of the A-exciton for RC band was fitted using the relation proposed by Rudin et al.[41] given as

$$FWHM(T) = \\ = W_0 + \beta T + \gamma/\left[\exp(\hbar\omega_{LO}/kT) - 1\right], \tag{2}$$

where W_0 is a width at T = 0K including also inhomogeneous broadening, β is a coefficient for the interaction of excitons with acoustic phonons and the last term represents the interaction with LO

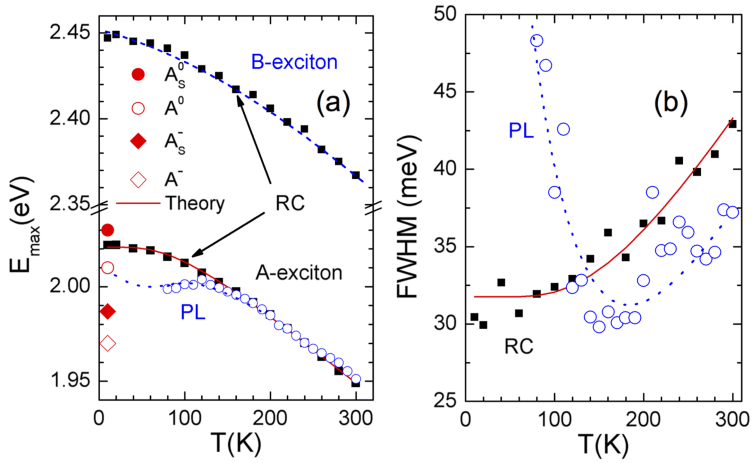

FIG. 7. (a) Temperature dependence of the PL peak energy (blue circles) and peak position of reflectance contrast (RC) spectra (solid squares). Fitting result using Eq. (1) is given with red curve. Peak positions of different PL peaks at T=10K are also indicated. (b) Temperature dependence of $FWHM$ of A^0-exciton peak obtained from RC (solid squares) and PL spectra (circles). Red curve represents the fitting with Eq. (2).

TABLE I. Fitting parameters as obtained from fitting of the temperature dependence of E_{max} and *FWHM* (RC spectra) for A^0-exciton peak using Eq. (1) and Eq. (2). Fitting results from Ref. 3 are given in parentheses.

Fitting equation	Parameter	Value
Eq. (1)	*E(0)* (eV)	2.021 (2.063)
	S	2.23 (2.4)
	$\hbar\omega$ (meV)	22.7 (31)
Eq. (2)	γ (meV)	53.2
	$\hbar\omega_{LO}$ (meV)	44.6
	W_0 (meV)	31.8

(longitudinal optical) phonons, $\hbar\omega_{LO}$ is the LO-phonon energy and is taken to be equal to 44.6 meV for WS_2.[42] The interaction with acoustic phonons was neglected because it is usually very small. The fitting result is presented in Fig. 7(b) as a red curve and fitting parameters are shown in Table I. At higher temperatures (T > 150K) the *FWHM* of PL band also shows widening due to electron-phonon interaction, but the width of the PL band seems to be smaller than for RC band. This difference is related to the fact, that the PL spectrum does not represent the total exciton density of states because photoexcited carriers undergo relaxation processes before they recombine radiatively. Therefore the PL spectrum corresponds to distribution of lowest exciton energy states while reflectance contrast spectrum represents the distribution of all exciton states. However, at temperatures T < 150K the width of the PL band starts to increase rapidly with decreasing of temperature. Moreover, the shape of the PL band near the peak maximum changes and becomes wider, see Fig. 6 (b). This behavior is again typical for localized excitons.[43]

C. Theory of localized excitons

A general model for the luminescence of localized-state ensemble (LSE) was given by Li et al.[43] According to this work the shape of PL band for localized excitons is asymmetric and can be calculated using density of states function for excitons $\rho(E)$ and a distribution function $f(E,T)$ for localized carriers. The $f(E,T)$ function has a shape resembling a Fermi distribution with a characteristic energy E_a. The distribution of the localized states $\rho(E)$ is usually assumed to be described by a Gaussian-like function, but other shapes are also possible. In Ref. 29, for example, the Lorentzian shape was used. According to Ref. 43, the low-energy side of PL band is less affected by the distribution function $f(E,T)$ and therefore the shape of this side gives a clue about the shape of $\rho(E)$ function. In our case it is reasonable to approximate function $\rho(E)$ by hyperbolic secant, because this function was the most suitable one for PL band shape fittings. Then the overall shape of localized excitons PL band is given by:

$$I(E,T) = A(T)\rho(E)f(E,T) = \\ = \frac{A(T)\rho_0 \mathrm{sech}\left[\frac{E-E_0}{\sigma}\right](\tau_{tr}/\tau_r)}{\exp\left[\frac{E-E_a}{kT}\right] + \tau_{tr}/\tau_r}, \quad (3)$$

where $A(T)$ is a temperature dependent term, ρ_0 is the amplitude, E_0 is a peak position and σ is a width of the density of states function, $1/\tau_r$ and $1/\tau_{tr}$ represent the rate of radiative recombination and the attempt-to-escape rate of the localized carriers, respectively. The shape calculated by Eq. (3) can be quite well fitted using an asymmetric hyperbolic secant function. At the same time, the shape and the temperature dependence of peak position E_{max} and *FWHM* of localized excitons band significantly depend on E_0 and E_a. In many cases[43] the best correlation with experimentally measured temperature dependencies is obtained by taking $E_0 > E_a$. Figure 8(a) shows calculated by using Eq. (3) PL spectra for the case E_0 - E_a = 20 meV, σ = 6 meV and τ_{tr}/τ_r = 0.1 and in Fig. 8(b) the temperature dependencies of peak position E_{max}-E_0 and *FWHM* are given. It can be seen that the shape of calculated PL band shows very similar behavior to what was observed experimentally, see Figs. 6–8. At temperatures T < 150K we see a rapid increase of *FWHM* and a gradual red-shift of peak position. Furthermore, the shape of the PL band nearthe peak maximum becomes wider

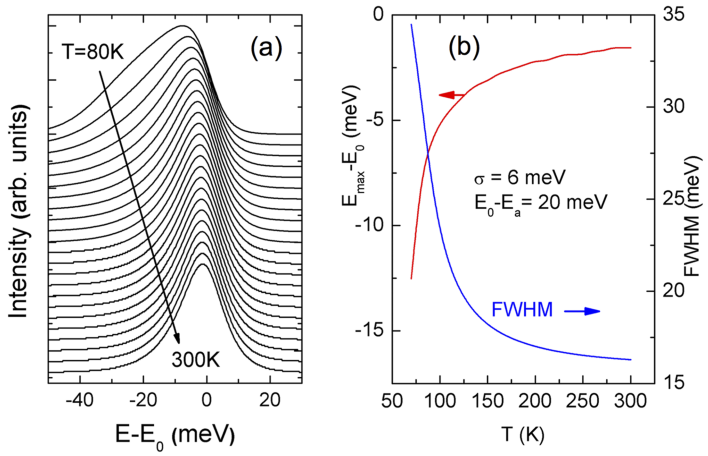

FIG. 8. (a) Calculated temperature dependence of luminescence peak shape (normalized) for the case of $E_0 - E_a = 20$ meV and σ = 6 meV using Eq. (3), (b) the temperature dependence of peak position (red) and FWHM (blue).

and the same trend was observed experimentally, see Fig. 6(b). This means that the LSE model applies to aged WS_2 monolayer and spatial fluctuations of the bandgap energy due to local strain will induce this localization in the lowest-energy regions, where excitons will be swept by the strain-induced potential gradient and funneled toward the center.[44] The LSE model was previously proposed also for WS_2 monolayers grown on a silicon substrate in a hot-wall furnace, where the room temperature PL peak has a maximum at about 1.955 eV.[45] One potential source of the local strain is associated to relatively high nanocaps found by AFM scan on a surface of WS_2 monolayer, see Fig. 1(c). The average distance between these nanocaps is less than the diffusion length of excitons in WS_2 monolayers (~350 nm[46]) and therefore excitons can be easily captured in these regions with high strain and reduced band gap energy. The possible strain ε for these nanocaps was obtained from the curvature of nanocaps using the pure-bending equation $\varepsilon = (d/2)/(R - d/2)$, where R and d are the radius of curvature and the thickness of WS_2 monolayer, respectively.[47] Taking the average thickness of the monolayer $d = 0.8$ nm, height $h = 7$ nm and the diameter $a = 30$ nm of nanocaps, the tensile strain value will be $\varepsilon = 2.1$ % and, according to experimentally determined peak position shift of –11.3 meV per % of strain,[5] the overall peak position shift is 23.7 meV. This obtained value is in good correlation with the A^0-exciton peak position separation between as-grown and aged WS_2 monolayers, see Fig. 3. At low temperatures we also detected additional exciton A_S^0 and trion A_S^- peaks at higher energies, see Fig. 4. The position of these peaks suggests that they are also related to strained areas, where the band gap energy is about 4 meV less than in as-grown monolayers. This energy corresponds to the strain value of $\varepsilon = 0.35\%$ and this strain could be caused by the general increase of the surface roughness in aged monolayers. These states are very shallow and excitons are easily thermalized into deeper states when temperature is increased. The whole aged monolayer surface is thus disturbed by the strain having slightly different origin (increased surface roughness vs. nanocaps) and value and therefore we could see emission from localized states only. The recombination model for excitons and trions in aged WS_2 monolayer is given in Fig. 9. At low temperatures the exciton and trion recombination is possible from both deep ρ_D and shallow ρ_S localized states showing double peak structure. At higher temperatures only ρ_D states are active. According to our calculations $\varepsilon_D = 24$ meV and $\varepsilon_S = 4$ meV.

The origin of nanocaps in aged monolayer is not clear. It was shown in Ref. 27 that aging usually leads to oxidation of metal states and this process is more prominent at grain boundaries. Sulfur vacancies are similarly believed to play important role in these oxidation processes. It is also possible, that very small nanoparticles were formed on a Si/SiO_2 surface during growth and they are not completely reacted in S atmosphere. Similar nanoparticles were found in many monolayers where they acted as seeds for CVD monolayer growth.[48] During aging these nanoparticles beneath the monolayer start to expand due to oxidation and, as a result, nanocaps are formed. But again, the true origin of these nanocaps is a topic of future studies.

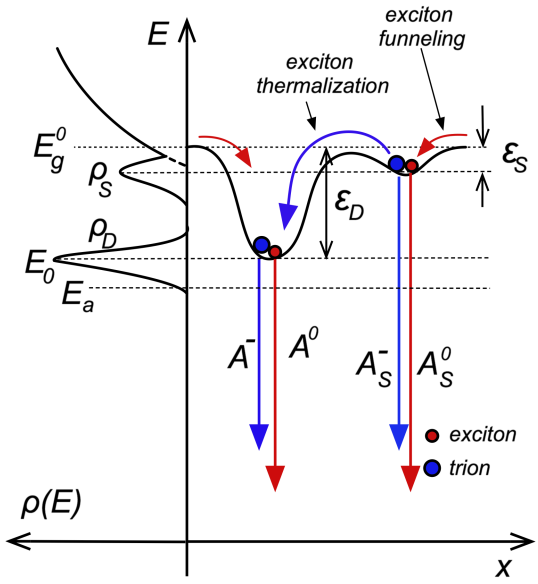

FIG. 9. Proposed recombination model for localized excitons and trions in aged WS_2 monolayers. Density of deep ρ_D and shallow ρ_S localized states are shown. The origin of double PL peaks is explained.

IV. CONCLUSIONS

We have presented photoluminescence and reflectance contrast spectra of aged WS_2 monolayers, measured at temperatures T=10-300K. Room temperature PL spectra show the A-exciton at 1.951 eV, while in as-grown monolayer the peak was at 24 meV higher energy. We propose that this red-shift is related to the band gap narrowing due to formation of nanocaps and local tensile strain. The local strain value related to nanocaps is about 2.1%. Additional weaker strain (~0.35%) is associated with increased surface roughness in aged monolayers. At T=10K double exciton and trion peaks were discovered and we suggest that they are present due to these different strains. In addition, a wide defect related exciton band X_D was found at about 1.93 eV in all aged monolayers. We showed that the theory of localized-state ensemble can be used to describe well the temperature dependence of peak position and halfwidth of the A-exciton band.

ACKNOWLEDGMENTS

This work was supported by institutional research funding IUT 19-28 and IUT 34-27 of the Estonian Ministry of Education and Research, by the European Union through the European Regional Development Fund (Project TK141), and by FP7 project CHEETAH, EC grant agreement no. 609788. Dr. R. Naidu is acknowledged for her help in AFM measurements.

[1] G. Bhimanapati, Z. Lin, V. Meunier, Y. Jung, J. Cha, S. Das, D. Xiao, Y. Son, M. S. Strano, V. R. Cooper, L. Liang, S. G. Louie, E. Ringe, W. Zhou, S. S. Kim, R. R. Naik, B. G. Sumpter, H. Terrones, F. Xia, Y. Wang, J. Terrones, and J. A. Robinson, ACS Nano **9**, 11509 (2015).
[2] H. Terrones, F. López-Urías, and M. Terrones, Sci. Rep. **3**, 1549 (2013).
[3] K. Wei, Y. Liu, H. Yang, X. Cheng, and T. Jiang, Appl. Opt. **55**, 6251 (2016).
[4] T. Kato and T. Kaneko, ASC Nano **10**, 9687 (2016).
[5] Y. Wang, C. Cong, W. Yang, J. Shang, N. Peimyoo, Y. Chen, J. Kang, J. Wang, W. Huang, and T. Yu, Nano Res. **8**, 2562 (2015).
[6] L. Yuan and L. Huang, Nanoscale **7**, 7402 (2015).
[7] A. McCreary, A. Berkdemir, J. Wang, M. A. Nguyen, A. L. Elías, N. Perea-López, K. Fujisawa, B. Kabius, V. Carozo, D. A. Cullen, T. E. Mallouk, J. Zhu, and M. Terrone, J. Mater. Res. **31**, 931 (2016).
[8] G. Plechinger, P. Nagler, A. Arora, R. Schmidt, A. Chernikov, A. Granados del Águila, P. C. M. Christianen, R. Bratschitsch, C. Schüller, and T. Korn, Nat. Commun. **7**, 12715 (2016).
[9] W. Zhao, Z. Ghorannevis, L. Chu, M. Toh, C. Kloc, P.-H. Tan, and G. Eda, ASC Nano **7**, 791 (2013).
[10] J. Shang, X. Shen, C. Cong, N. Peimyoo, B. Cao, M. Eginligil, and T. Yu, ASC Nano **9**, 647 (2015).
[11] G. Plechinger, P. Nagler, J. Kraus, N. Paradiso, C. Strunk, C. Schüller, and T. Korn, Phys. Status Solidi RRL **9**, 457 (2015).

[12] Y. Gong, Z. Lin, G. Ye, G. Shi, S. Feng, Y. Lei, A. L. Elías, N. Perea- López, R. Vajtai, H. Terrones, Z. Liu, M. Terrones, and P. M. Ajayan, ASC Nano **9**, 11658 (2015).
[13] A. M. Rivera, A. P. S. Gaur, S. Sahoo, and R. S. Katiyar, J. Appl. Phys. **120**, 105102 (2016).
[14] P. K. Chow, R. B. Jacobs-Gedrim, J. Gao, T.-M. Lu, B. Yu, H. Terrones, and N. Koratkar, ASC Nano **9**, 1520 (2015).
[15] A. T. Hanbickia, M. Curriea, G. Kioseogloub, A. L. Friedmana, and B. T. Jonker, Solid State Commun. **203**, 16 (2015).
[16] D. W. Latzke, W. Zhang, A. Suslu, T.-R. Chang, H. Lin, H.-T. Jeng, S. Tongay, J. Wu, A. Bansil, and A. Lanzara, Phys. Rev. B **91**, 235202 (2015).
[17] L. Su, Y. Yu, L. Cao, and Y. Zhang, Nano Res. **8**, 2686 (2015).
[18] Y. Yu, Y. Yu, C. Xu, Y.-Q. Cai, L. Su, Y. Zhang, Y.-W. Zhang, K. Gundogdu, and L. Cao, Adv. Funct. Mater. **26**, 4733 (2016).
[19] L. Meng, Y. Zhang, S. Hu, X. Wang, C. Liu, Y. Guo, X. Wang, and X. Yan, Appl. Phys. Lett. **108**, 263104 (2016).
[20] H. Li, A. W. Contryman, X. Qian, S. M. Ardakani, Y. Gong, X. Wang, J. M. Weisse, C. H. Lee, J. Zhao, P. M. Ajayan, J. Li, H. C. Manoharan, and X. Zheng, Nat. Commun. **6**, 7381 (2015).
[21] A. Castellanos-Gomez, R. Roldan, E. Cappelluti, M. Buscema, F. Guinea, H. S. J. van der Zant, and G. A. Steel, Nano Lett. **13**, 5361 (2013).
[22] Q. Zhang, Z. Chang, G. Xu, Z. Wang, Y. Zhang, Z.-Q. Xu, S. Chen, Q. Bao, J. Z. Liu, Y.-W. Mai, W. Duan, M. S. Fuhrer, and C. Zheng, Adv. Funct. Mater. **26**, 8707 (2016).
[23] I. Paradisanos, N. Pliatsikas, P. Patsalas, C. Fotakis, E. Kymakis, G. Kioseoglou, and E. Stratakis, Nanoscale **8**, 16197 (2016).
[24] Y.-H. Lee, L. Yu, H. Wang, W. Fang, X. Ling, Y. Shi, C.-T. Lin, J.-K. Huang, M.-T. Chang, C.-S. Chang, M. Dresselhaus, T. Palacios, L.-J. Li, and J. Kong, Nano Lett. **13**, 1852 (2013).
[25] T. Georgiou, H. Yang, R. Jalil, J. Chapman, K. S. Novoselova, and A. Mishchenko, Dalton Trans. **43**, 10388 (2014).
[26] H. Liu, J. Lu, K. Ho, Z. Hu, Z. Dang, A. Carvalho, H. R. Tan, E. S. Tok, and C. H. Sow, Nano Lett. **16**, 5559 (2016).
[27] J. Gao, B. Li, J. Tan, P. Chow, T.-M. Lu, and N. Koratkar, ACS Nano **10**, 2628 (2016).
[28] Y. Rong, K. He, M. Pacios, A. W. Robertson, H. Bhaskaran, and J. H. Warner, ASC Nano **9**, 3695 (2015).
[29] J. Krustok, T. Raadik, R. Jaaniso, V. Kiisk, I. Sildos, M. Marandi, H.-P. Komsa, B. Li, X. Zhang, Y. Gong, and P. M. Ajayan, Appl. Phys. Lett. **109**, 253106 (2016).
[30] A. Berkdemir, H. R. Gutiérrez, A. R. Botello-Méndez, N. Perea-López, A. L. Elías, C.-I. Chia, B. Wang, V.H. Crespi, F. López -Urías, J.-C. Charlier, H. Terrones, and M. Terrones, Sci. Rep. **3**, 1755 (2013).
[31] C. Cong, J. Shang, X. Wu, B. Cao, N. Peimyoo, C. Qiu, L. Sun, and T. Yu, Adv. Opt. Mater. **2**, 131 (2014).
[32] H. R. Gutiérrez, N. Perea- López, A. L. Elías, A. Berkdemir, B. Wang, R. Lv, F. López -Urías, V. H. Crespi, H. Terrones, and M. Terrones, Nano Lett. **13**, 3447 (2013).
[33] X. Zhang, X.-F. Qiao, W. Shi, J.-B. Wu, D.-S. Jiang, and P.-H. Tan, Chem. Soc. Rev. **44**, 2757 (2015).
[34] Y. Dinga and B. Xiao, RSC Adv. **5**, 18391 (2015).
[35] J. S. Ross, S. Wu, H. Yu, N. J. Ghimire, A. M. Jones, G. Aivazian, J. Yan, D. G. Mandrus, D. Xiao, W. Yao, and X. Xu, Nat. Commun. **4**, 1474 (2013).
[36] S. Tongay, J. Suh, C. Ataca, W. Fan, A. Luce, J. S. Kang, J. Liu, C. Ko, R. Raghunathanan, J. Zhou, F. Ogletree, J. Li, J. C. Grossman, and J. Wu, Sci. Rep. **3**, 2657 (2013).
[37] A. Arora, M. Koperski, K. Nogajewski, J. Marcus, C. Faugeras, and M. Potemski, Nanoscale **7**, 10421 (2015).
[38] K. P. O'Donnell and X. Chen, Appl. Phys. Lett. **58**, 2924 (1991).
[39] A. R. Mohmad, F. Bastiman, C. J. Hunter, R. D. Richards, S. J. Sweeney, J. S. Ng, J. P. R. David, and B. Y. Majlis, Phys. Status Solidi B **251**, 1276 (2014).
[40] Q. Li, S. J. Xu, W. C. Cheng, M. H. Xie, S. Y. Tong, C. M. Che, and H. Yang, Appl. Phys. Lett. **79**, 1810 (2001).
[41] S. Rudin, T. L. Reinecke, and B. Segall, Phys. Rev. B **42**, 11218 (1990).
[42] A. Molina-Sánchez and L. Wirtz, Phys. Rev. B **84**, 155413 (2011).
[43] Q. Li, S. J. Xu, M. H. Xie, and S. Y. Tong, Europhys. Lett. **71**, 994 (2005).
[44] J. Feng, X. Qian, C.-W. Huang, and J. Li, Nat. Photonics **6**, 866 (2012).
[45] X. H. Wang, J. Q. Ning, Z. C. Su, C. C. Zheng, B. R. Zhu, L. Xie, H. S. Wu, and S. J. Xu, RSC Adv. **6**, 27677 (2016).
[46] J. He, D. He, Y. Wang, Q. Cui, F. Ceballos, and H. Zhao, Nanoscale **7**, 9526 (2015).
[47] B. G. Shin, G. H. Han, S. J. Yun, H. M. Oh, J. J. Bae, Y. J. Song, C.-Y. Park, and Y. H. Lee, Adv. Mater. **28**, 9378 (2016).
[48] J. D. Cain, F. Shi, J. Wu, and V. P. Dravid, ACS Nano **10**, 5440 (2016).